RSC Advances

PAPER

View Article Online
View Journal | View Issue

Cite this: *RSC Adv.*, 2021, **11**, 29590

A simple electrochemical sensor based on rGO/MoS_2/CS modified GCE for highly sensitive detection of Pb(II) in tobacco leaves†

Chuanen Guo,[a] Chengxiang Wang,[b] Hongyan Sun,[b] Dongmei Dai[b] and Hongtao Gao *[b]

High-performance electrode modification materials play a crucial role in improving the sensitivity of sensor detection in electrochemical determination of heavy metals. In this study, a rGO/MoS_2/CS nanocomposite modified glassy carbon electrode (GCE) was used to construct a sensitive sensor for detecting lead ions in tobacco leaves. The reduced graphene oxide (rGO) was used to increase the conductivity of the sensor, and the nano-flowered MoS_2 could provide a large reaction specific surface area and a certain active site for heavy metal reaction. Chitosan (CS) was used to improve the enrichment ability of heavy metals and increase the electrocatalytic activity of electrode. Thus, an electrochemical sensor with excellent performance in reproducibility, stability and anti-interference ability was established. The stripping behavior of Pb(II) and the application conditions of the sensor were studied by square wave anodic stripping voltammetry (SWASV). The investigation indicated that the sensor exhibited high detection sensitivity in the range of 0.005–0.05–2.0 μM, and the limit of detection (LOD) was 0.0016 μM. This work can provide a fast and effective method for determination of Pb(II) in samples with low content, such as tobacco leaves.

Received 12th July 2021
Accepted 16th August 2021

DOI: 10.1039/d1ra05350g

rsc.li/rsc-advances

1. Introduction

Heavy metals are widely distributed in the earth's crust, but anthropogenic activities such as mining and industry contribute to the enrichment of these substances in foods and make their contents exceed the safe range. In view of the potential threat of heavy metals in the natural environment and food, heavy metal pollution has received widespread attention.[1] Since tobacco plants can effectively extract metals from the ground, it is sometimes used to repair metal-contaminated soil and groundwater.[2,3] Residues of heavy metals may be caused by external environmental pollution, such as non-ferrous metal smelting, factory emissions, and the use of leaded gasoline, which permeate the production and preservation stage of tobacco through incorrect procedures.[4,5] The use of metal-containing fertilizers, herbicides, lead arsenate and other pesticides in the cultivation of commercial tobacco, as well as metal tools for growing, drying and roasting tobacco further increase the heavy metal Pb(II) content in the tobacco leaves, makes the cigarettes ultimately contain a non-negligible Pb(II) concentration.[6,7] And excessive amounts of heavy metals in tobacco will pose a risk to tobacco users. Hence, it is extremely urgent to develop a rapid and sensitive method for the detection of heavy metal, such as Pb(II) in tobacco leaves.

Some highly sensitive spectroscopic techniques, including atomic absorption spectrometry (AAS),[8] X-ray fluorescence spectrometry (XFS),[9] and inductively coupled plasma mass spectrometry (ICP-MS),[10] are stable and commonly used methods to determine Pb(II). However, the disadvantages of these techniques, including complex analytical procedures, expensive instruments and lengthy sample processing, hinder their practical application. Square wave anodic stripping voltammetry (SWASV), as a classic electrochemical technique, has attracted much attention due to its high sensitivity for simultaneous analysis of various heavy metal ions.[11,12] At present, the sensitivity of SWASV depends largely on the improvement of modified electrode materials. In the last decade, many substances used as modifiers, such as nanomaterials,[13] complexes,[14] carbon-based materials[15–17] and so on, have been found in the development of electrochemical sensors. These modifiers contributed to improved conductivity, specific surface area and sensitivity, which enabled SWASV appear as an alternative method with lower detection limit to replace traditional analytical methods.

Carbon based materials, such as mesoporous carbon,[15] carbon nanotubes,[16] graphene,[17] and fullerenes,[18] have attracted

[a]Judicial Expertise Center, Shandong University of Political Science and Law, Jinan, 250014, P. R. China. E-mail: 000807@sdupsl.edu.cn

[b]Key Laboratory of Optic-electric Sensing and Analytical Chemistry for Life Science, MOE, Qingdao University of Science & Technology, Qingdao, 266042, P. R. China. E-mail: gaohtao@qust.edu.cn; Fax: +86-0532-84022990; Tel: +86-0532-84022990

† Electronic supplementary information (ESI) available. See DOI: 10.1039/d1ra05350g

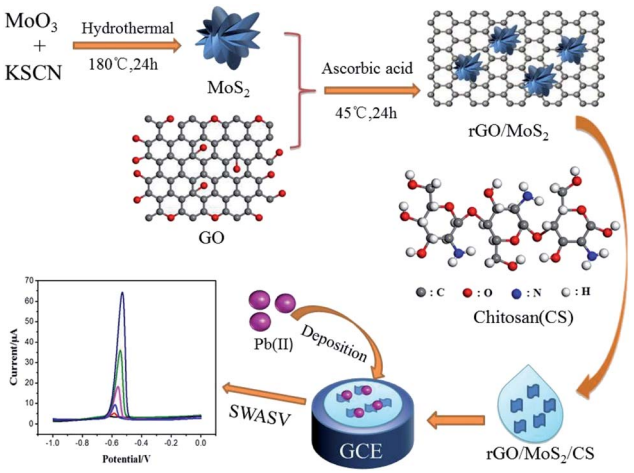

Scheme 1 Schematic diagram of the constructed sensor based on GCE modified with rGO/MoS_2/CS and electrochemical analysis process for Pb(II). SWASV is the abbreviation of Square wave anodic stripping voltammetry.

extensive attention due to their unique properties. Among all advanced carbon materials, graphene is a well-known two-dimensional (2D) single-layer structure with a high theoretical specific surface area (2620–2700 $m^2\ g^{-1}$). It also has attractive properties such as tunable band gap, good biocompatibility and electron transfer capability. Therefore, graphene and graphene-based composites have been used to detect trace amounts of heavy metal ions, organic compounds, biomolecules and drugs.[19,20] However, graphene has poor stability and is easy to agglomerate in aqueous solution. Various materials, such as multifunctional biomolecules,[21] natural biopolymers,[22] metal oxides[23] and biological enzymes,[24] have been used to prevent re-deposition of graphene. As a natural polymer material containing nitrogen and oxygen, chitosan (CS) can provide a large number of functional groups for carbon nanostructures, which can improve the stability and application range of grapheme.[25] Not to mention CS has many advantages, such as good biocompatibility, high electrical conductivity, excellent chemical stability, film forming ability and so on.[26] Therefore, CS might improve the induction of graphene to target metal ions. Molybdenum sulfide (MoS_2) has an inherent sulfur-rich surface,[27] which own distinctive properties, including large surface area, excellent mechanical flexibility, excellent chemical and thermal stability. MoS_2 has a promising application, especially in combination with graphene-based materials as a viable alternative to heavy metal adsorption and detection.[28,29]

In this work, a simple electrochemical sensor based on GCE modified with rGO/MoS_2/CS was constructed for high-sensitive determination of Pb(II) in tobacco leaves. Ascorbic acid was originally used as a reducing agent to reduce graphene oxide (GO) in a mild, simple, environmentally friendly and efficient reduction process while complexing with hydrothermally prepared MoS_2. Then, it was dispersed in water together with CS to prepare an electrode modification liquid, and the whole process was simple and effective. The test for actual tobacco leaves proved that the scheme was an effective method for detecting Pb(II). The whole process of the constructed sensor based on GCE modified with rGO/MoS_2/CS and electrochemical determination for Pb(II) have been shown in Scheme 1.

2. Experimental section

2.1 Regents

Molybdenum trioxide (MoO_3), potassium thiocyanate (KSCN) and lead nitrate ($Pb(NO_3)_2$) were available from Tianjin Guangcheng Chemical Reagent Co., Ltd. Sodium acetate (CH_3COONa, NaAc), glacial acetic acid (CH_3COOH, HAc), concentrated nitric acid, potassium chloride (KCl), potassium ferrocyanide trihydrate ($K_4Fe(CN)_6\cdot 3H_2O$) and potassium hexacyanoferrate ($K_3Fe(CN)_6$) were available from Sinopharm Chemical Reagent Co., Ltd. Ascorbic acid and chitosan (CS) were bought from Aladdin Industral Corporation. All the above chemicals and reagents were of analytical grade and were used without further purification.

2.2 Instrumentation

The surface morphologies of samples were characterized by scanning electron microscopy (SEM, JSM-6300, JEOL Ltd, Japan) and transmission electron microscope JEM-2100 (JEOL Ltd, Japan). XRD patterns were recorded using a Bruker D8 Advance X-ray diffractometer to determine the crystalline phase of the nanomaterials. Ultrasonic cleaner (JY92-IIN) was purchased from Ningbo Xinzhi Biotechnology Co., Ltd. The concentration of Pb(II) in tobacco leaves sample was determined by ICP-MS (Thermo, X-series ICP-MS). Fourier Transform Infrared (FTIR, Nicolet iS5, USA) was used to analyze functional group status of the prepared materials. All electrochemical experiments were carried out on CHI660E electrochemical workstation (ChenHua Instruments Co., Shanghai, China). The bare glassy carbon electrode (GCE, diameter 3 mm) or modified GCE was the working electrode; the platinum electrode was used as the counter electrode, and the saturated Ag/AgCl electrode was used as the reference electrode to complete the standard three-electrode system.

2.3 Synthesis of MoS_2 composite

A certain amount of MoO_3 (*ca.* 2.50 mmoL) and KSCN (*ca.* 6.25 mmoL) were dissolved in 30 mL of deionized water, and were put in ultrasonic cleaner for 30 min to obtain the gray uniform precursor solution. The precursor solution was then transferred to a Teflon-lined reaction kettle and placed in constant temperature drying oven at 180 °C for 12 h. The reaction vessel was naturally cooled to room temperature. The sample was washed with ultrapure water and ethanol repeatedly by centrifugation, and dried at 60 °C for 8 h to obtain the black powder product.

2.4 Synthesis of rGO/MoS_2 composite

Graphene oxide (GO) was prepared by the classical Hummer method. 0.10 g of GO was uniformly dispersed into 100 mL of deionized water, which was mixed with the MoS_2 suspension (1 mg mL^{-1}, ~30 mL) prepared in the previous step. A certain

amount of ascorbic acid[30] was added under agitation, the solution was then shaken for 8 h at 45 °C. After composite was formed, it was washed successively three times with ultrapure water and ethanol. Finally, the dark rGO/MoS_2 was obtained after dried in vacuum drying box at 60 °C for 8 h.

2.5 Electrode modification

The exposed surface of glassy carbon electrode (GCE) was sequentially polished with 1.0, 0.3, and 0.05 μm of alumina powder successively. And after then, ultrasonic washing was carried out for 1 min with absolute ethanol and ultrapure water, followed by blow drying with nitrogen.

The process of GCE modification was as follows: 0.02 g of the prepared composite was added to 20.00 mL of ultrapure water for a short period of sonication for 10 min; then 0.30 mL of glacial acetic acid and 0.02 g of CS were added separately under stirring, followed by sonication for 10 minutes to obtain a uniform and stable suspension. Then, 6.00 μL of the above suspension was dropped on the surface of GCE, which was then dried using an infrared lamp. Finally, a sensor based on GCE modified with rGO/MoS_2/CS (rGO/MoS_2/CS/GCE) was constructed.

3. Results and discussion

3.1 Characterization of material

3.1.1. Morphology observations. The surface morphologies of the samples were characterized by SEM and TEM, respectively. Fig. 1a presented SEM image of MoS_2, which could be seen that the MoS_2 had a uniform spherical flower-like structure. Fig. 1b showed the SEM image of rGO/MoS_2, which indicated the flower-like MoS_2 was attached to the wrinkle flakes rGO. Fig. 1c showed the surface morphology of rGO/MoS_2/CS, which illustrated that the composite was distributed uniformly due to the adhesive effect of chitosan. Fig. 1d was TEM image of rGO/MoS_2, which verified MoS_2 has attached on the network of rGO with uniform thickness. After combination of CS, the surface of rGO/MoS_2 was covered with a thicker layer of material, which was presented in Fig. 1e.

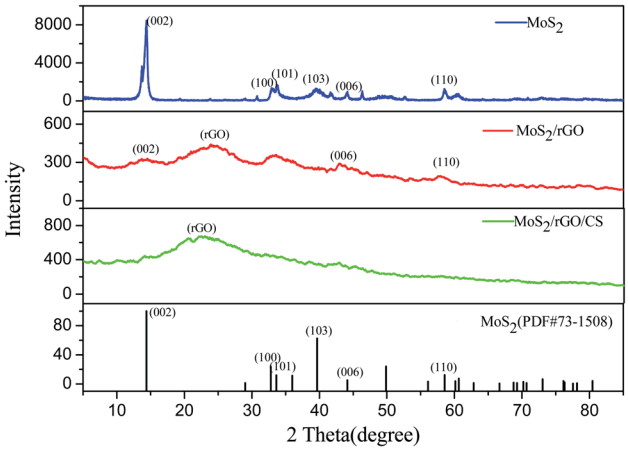

Fig. 2 XRD pattern of MoS_2, rGO/MoS_2, rGO/MoS_2/CS.

3.1.2. Crystalline phases characterization. It is well known that X-ray powder diffraction (XRD) is an effective mean to characterize the structural and crystalline phases of samples. The XRD patterns of MoS_2, rGO/MoS_2 and rGO/MoS_2/CS were presented in Fig. 2. The peaks located at 14.3°, 32.8°, 33.7°, 39.6°, 44.1° and 58.5° corresponding to the (002), (100), (101), (103), (006) and (110) planes of MoS_2 (PDF #73-1508) could be clearly found from the XRD pattern, showing the successful preparation of MoS_2. The XRD pattern of MoS_2/rGO showed that the characteristic peak intensity of MoS_2 was weakened after composited with rGO, but the corresponding peak could still be found. However, after compositing with CS, the characteristic peak of MoS_2 disappeared. This reason was that the surface of the material was covered with a film by the addition of CS,

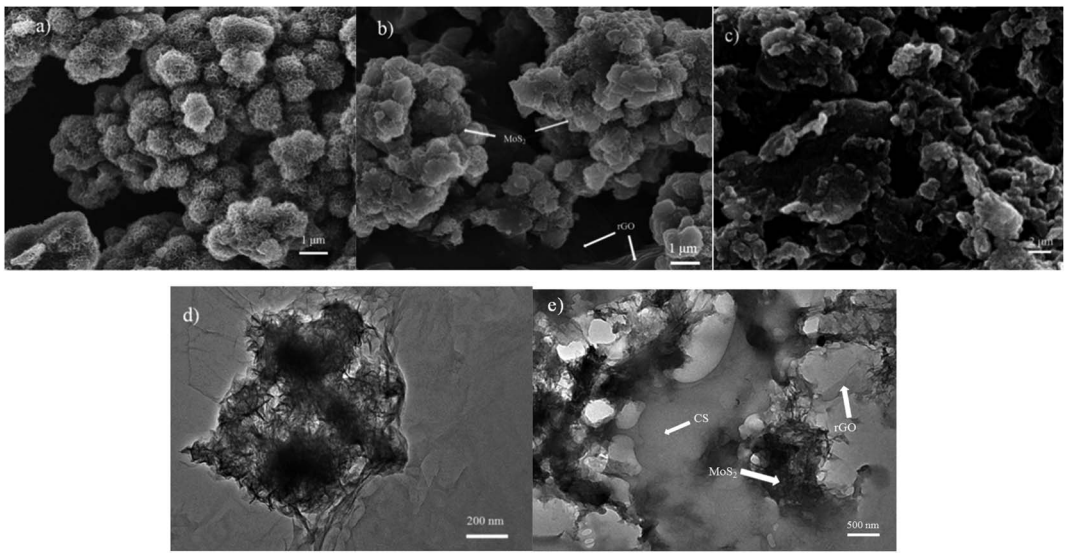

Fig. 1 The SEM images of (a) MoS_2, (b) rGO/MoS_2, (c) rGO/MoS_2/CS, and the TEM images of (d) rGO/MoS_2, (e) rGO/MoS_2/CS.

which masked the surface structure of the original material. This resulted corresponded to the results of both SEM and TEM.

3.1.3. FT-IR analysis. The FT-IR spectra of samples were shown in Fig. S1†. It was observed that the characteristic adsorptions from oxygen-containing function groups in spectrum of GO. For example, the peak at 3441 cm^{-1} could be assigned to the stretching vibration and deformation vibration of O–H, the peak at 1731 cm^{-1} belonged to the C=O, while the peaks at both 1636 and 1065 cm^{-1} were the stretching vibration peaks of C–O.[31,32] Compared with GO, the characteristic peak of oxygen-containing functional group in rGO/MoS_2 was significantly reduced, indicating that the degree of GO reduction was better. The peak at 1401 cm^{-1} was ascribed to the peak of MoS_2, indicating that MoS_2 was successfully combined into the material.[33] As could be seen from the spectrum of rGO/MoS_2/CS, both the peak of N–H at 883 cm^{-1} and the peak of C–N at 1149 cm^{-1} indicated a successful recombination of CS[32] in the composite material.

3.2 Electrochemical behavior of modified electrode

The electrochemical properties of samples were characterized by cyclic voltammetry. Fig. 3a showed the cyclic voltammetry (CV) response of bare GCE, GO/MoS_2/GCE, rGO/MoS_2/GCE and rGO/MoS_2/CS/GCE electrodes in the solution containing $[Fe(CN)_6]^{3-/4-}$ (1.0 mM) and KCl (0.10 M) at a scan rate of 0.1 V s^{-1}. It could be seen from the figure that all the CV curves exhibited relatively symmetrical redox peaks, indicating that electrodes modified with these materials had all good reversibility in the redox process. Compared with GO/MoS_2/GCE, rGO/MoS_2/GCE had a larger redox peak current, which indicated that rGO had a better effect than GO in promoting the electron transfer process at the GCE surface. And the addition of CS further increased the peak current, which indicated that it helped to improve not only chemical stability but also electrochemical catalytic activity of the modified electrode.

Electrochemical impedance spectroscopy (EIS) was used to characterize the electrode interface properties of different materials.[34] Fig. 3b showed the Nyquist diagram of rGO/MoS_2/CS/GCE electrodes in the solution containing $[Fe(CN)_6]^{3-/4-}$ (1.0 mM) and KCl (0.10 M). As shown in Fig. 3b, the resistance of the GO/MoS_2 modified electrode was much larger than that of the bare electrode, because GO was weaker than rGO in electron transport. And at the same time, nanoflower-like MoS_2 did not have good performance in conductive efficiency. The rGO/MoS_2/GCE showed smaller electron transfer resistance. And after addition of CS, the resistance reduced further. These results meant that rGO promoted the electron transfer process at the surface of modified electrode, meanwhile CS helped to improve its electrochemical catalytic activity. These EIS results concurred with CV plots.

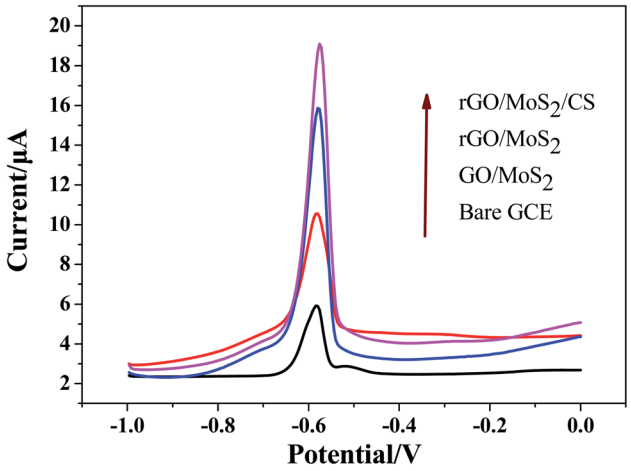

Fig. 4 SWASV response for bare GCE, GO/MoS_2/GCE, rGO/MoS_2/GCE and rGO/MoS_2/CS/GCE in 0.10 M HAc–NaAc (pH = 5.0) containing 0.50 μM of Pb(II). Under the conditions: deposition potential −1.3 V, deposition time 180 s, step potential 4 mV, amplitude 25 mV, frequency 25 Hz.

In order to evaluate the response ability of modified electrodes to Pb(II), experiments were conducted on electrodes modified with different materials by SWASV method. SWASV behaviors of Pb^{2+} at bare GCE, GO/MoS_2/GCE, rGO/MoS_2/GCE and rGO/MoS_2/CS/GCE had been studied in 0.10 M HAc–NaAc (pH = 5.0) with the potential range from −1.0 to 0.0 V, as shown in Fig. 4. The results showed that the modified electrodes used in this work had different degrees of improvement compared to

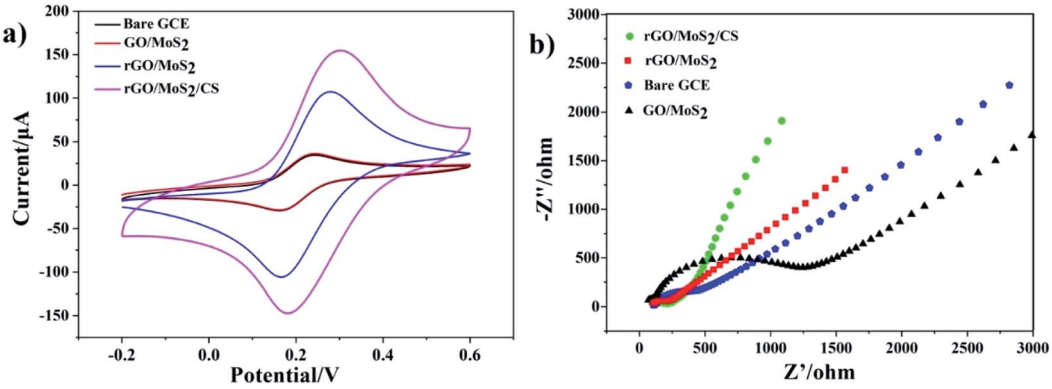

Fig. 3 (a) Cyclic voltammetry curves and (b) typical Nyquist plots of bare GCE, GO/MoS_2/GCE, rGO/MoS_2/GCE and rGO/MoS_2/CS/GCE in the solution containing $[Fe(CN)_6]^{3-/4-}$ (1.0 mM) and KCl (0.10 M).

the bare GCE. The small increasing in the peak current signal of the GO/MoS_2/GCE was mainly due to the poor electron transport capability of the system, which was not conducive to the redox reaction of Pb(II) on the electrode surface. The peak current signals generated by both rGO/MoS_2/GCE and rGO/MoS_2/CS/GCE were significantly improved, indicating that rGO had a good effect on improving the detection of Pb(II). Especially after the addition of CS, the peak current signal was increased by more than 5 times compared to that of bare GCE. This was mainly because CS had abundant functional groups (–NH_2, –OH, *etc.*) to facilitate the enrichment of Pb(II), thereby further improving the sensitivity of Pb(II) detection.

3.3 Optimization of experimental conditions

3.3.1. Optimization of modified materials. In order to obtain the maximum response signal of heavy metal ions in rGO/MoS_2/CS/GCE, the performance of electrode modification materials, such as CS content and ratio of MoS_2 to rGO, was first optimized. All measurements were performed to determine 0.50 μM Pb(II) by SWASV method. The experimental results were shown in Fig. S2.†

In this experiment, the content of CS was first optimized, which was illustrated in Fig. S2a.† The addition of CS was beneficial to the increase of peak current, but CS was easy to absorb and swell due to its water solubility. Excessive CS increased the thickness of the electrode modification material, which was not conducive to electron transport, thus affecting sensitivity of the sensor. It indicated that the CS content of 1.0 mg mL^{-1} corresponded to the peak current as the maximum response value.

The catalytical active site on the surface of MoS_2 facilitated the redox reaction in detection process, but its poor electron transporting ability had an opposite effect on the redox reaction. Since rGO not only increased the reaction surface area but also improved the electron transport efficiency of the electrode, so it was necessary to optimize the ratio of MoS_2 to rGO, which was shown in Fig. S2b.† When the ratio of MoS_2 to rGO is 3 : 10, the modified GCE had the best current response.

In summary, the concentration of CS was 1.0 mg mL^{-1} and the ratio of MoS_2 to rGO was 3 : 10 in the construction of sensor based on GCE.

3.3.2. Optimization of electrode operating conditions. The operating experimental conditions of electrode were optimized, such as pH, deposition potential, and deposition time. All measurements were performed to determine 0.50 μM Pb(II) by SWASV method. The experimental results were presented in Fig. S3.†

The HAc–NaAc buffer solution was the most suitable electrolyte solution for the determination of heavy metal, since it had the least competition for ion exchange centers on the electrode surface.[35] However, the pH of buffer solution had a great influence on the detection results. Therefore, the electrochemical responses of rGO/MoS_2/CS/GCE sensor for Pb(II) in 0.10 M HAc–NaAc buffer solution with pH 3.0–6.0 were investigated. Fig. S3a† presented the dissolution peak current and potential curves for Pb(II) in 0.10 M HAc–NaAc buffer solution with different pH, and the inset showed peak current plot with various pH. It showed a large shift in the dissolution peak potential at different pH, which was related to the presence of Pb(II) at different pH. At the same time, it could be seen that the peak current was correspondingly maximum under the condition of pH = 5.0, and the peak potential of dissolution was −0.58 V, which was consistent with the experimental result (Fig. 4). Therefore, 0.10 M HAc–NaAc buffer solution (pH = 5.0) was chosen as an optimal operating condition.

Since it might cause unwanted dissolution or oxide formation on the electrode surface, the appropriate electrode potential should be tested in experimental work. It could be seen from Fig. S3b,† the peak current of dissolution increased with the deposition potential reducing (between −1.0 V and −1.3 V). Excessively negative deposition potential led to the reduction of hydrogen and generation of H_2 on the surface of the electrode, which was not conducive to the detection repeatability. So, no experimental test was conducted under the condition of lower dissolution potential and −1.3 V was chosen as the deposition potential.

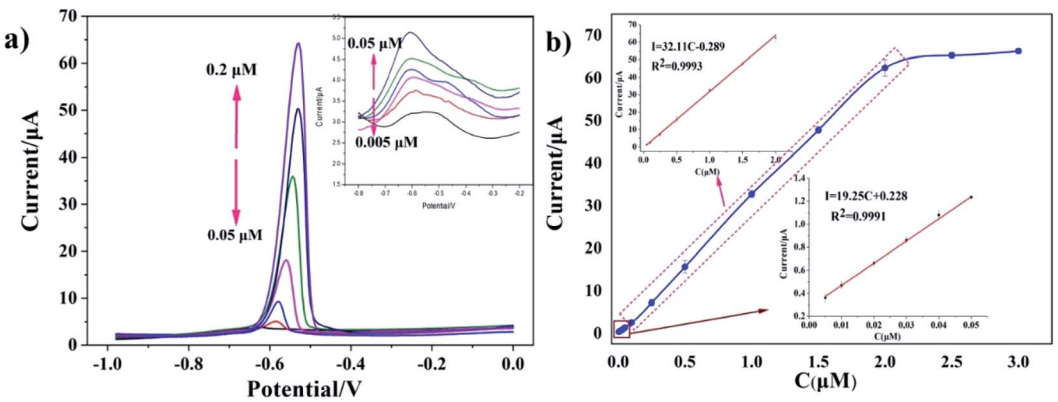

Fig. 5 (a) SWASV curves of the rGO/MoS_2/CS/GCE for Pb(II) detection in the range of 0.005 to 2.0 μM in 0.10 M NaAc–HAc (pH = 5.0) solution, the inset in a was dissolution peak currents in the range of 0.005 to 0.05 μM. (b) Corresponding calibration curves, the inset in b was calibration curve in the range from 0.005 to 2.0 μM and range from 0.005 to 0.05 μM under optimized operating conditions.

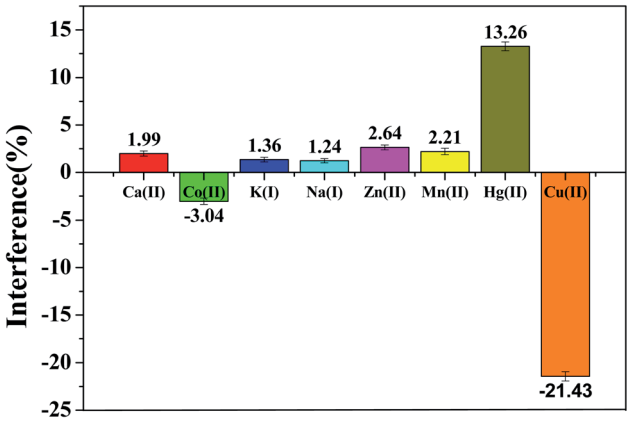

Fig. 6 Interference study of 100-fold other ions (Ca(II), Co(II), K(I), Na(I), Zn(II), Mn(II)) and 10-fold Cu(II), Hg(II) in the electrochemical determination of 0.50 μM Pb(II). Experimental conditions were consistent with Fig. 5.

The deposition time also played an important role in sensitivity and limit of detection during the stripping analysis of heavy metal ions. Excessive deposition time contributed to the evolution of hydrogen at the electrodes, limited the availability of active sites on the electrode surface, and interfered with the transmission quality of heavy metal ion deposition processes. Fig. S3c† showed the peak current varied with deposition time from 120 to 240 s. At 180 s, the dissolution current reached a large corresponding value. And longer deposition time did not significantly increase the peak current value. Thus 180 s was finally selected as the deposition time.

3.4 Electrochemical sensing for detecting Pb(II)

Under optimal experimental conditions, the SWASV responses of the rGO/MoS_2/CS/GCE to various concentrations of Pb(II) were shown in Fig. 5a. Fig. 5a showed the dissolution peak currents of Pb(II) with dissolution peak potential of −0.58 V, which indicated that dissolution peak increased with the increasing concentration. The inset in Fig. 5a presented the dissolution peak currents with concentration of Pb(II) varied from 0.005 μM to 0.05 μM. The corresponding calibration curve was presented in Fig. 5b, it could be seen from the figure that the response signal increase was not obvious when the concentration exceeded 2.0 μM. The reason for this result might be that Pb(II) on the surface of the electrode was in a relatively saturated state. So the linear equation of I (μA) = 32.11c (μM) −0.289 (R^2 = 0.9993) was plotted, which was applied for concentration of Pb(II) in the range from 0.05 to 2.0 μM with the sensitivity of the obtained Pb(II) was 32.11 μA μM^{-1}. The linear equation of I (μA) = 19.25c (μM) + 0.228 (R^2 = 0.9991) was obtained when low concentration of Pb(II) in the range of 0.005–0.05 μM. And the limit of detection (LOD) was calculated to be 0.0016 μM (0.33 ppb, 3σ method).

3.5 Interference and reproducibility studies

Mutual interference is a general matter existing in detection of several metal ions coexisted. Therefore, we discussed the interference from other ions at rGO/MoS_2/CS/GCE. The SWASV response of 0.50 μM Pb(II) was detected by adding 100 times of target ion (Ca(II), Co(II), K(I), Na(I), Zn(II), Mn(II)) under the optimum conditions. As showed in Fig. 6, the interfere from various ions to Pb(II) determination was presented by the relative standard deviation. The results showed that the main cations had a system impact of 3.04% or less, indicating that the sensor had good anti-interference ability. At the same time, it was also shown that 10 times Cu(II) had a great influence on the detection, which reduced the peak current by 21.43%. It could be explained by Cu(II) competing with the target ion for the surface active site of the electrode. The solution could reduce the influence of Cu(II) by adding a certain amount of ferricyanide to the actual sample extract before the measurement to form an insoluble and stable copper–iron cyanide complex with the help of the ligand.[36] In contrast, Hg(II) could be reduced to an amalgam, making Pb(II) easy to reduce, resulting in enhanced dissolution peak current. As shown in the Fig. 7a, the addition of 10 times Hg(II) increased the peak current by more than 15%. In fact, the presence of Hg(II) enhanced the sensitivity of detecting Pb(II) because a mercury film was formed, followed by formation of a metal hydride intermetallic compound on the electrode surface.[37]

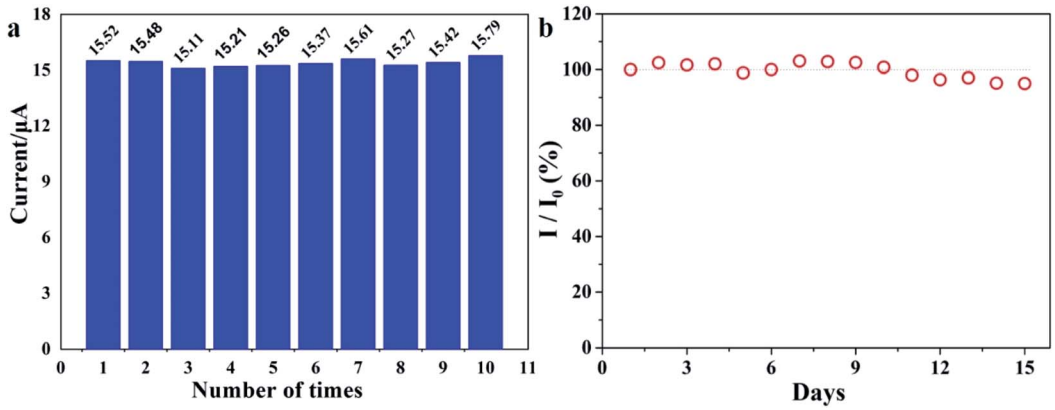

Fig. 7 (a) Reproducibility measurements repeated ten times using the rGO/MoS_2/CS/GCE. (b) Sensor response to Pb(II) (0.5 μM) recorded every day. The sensors are stored at 25 °C for 15 days.

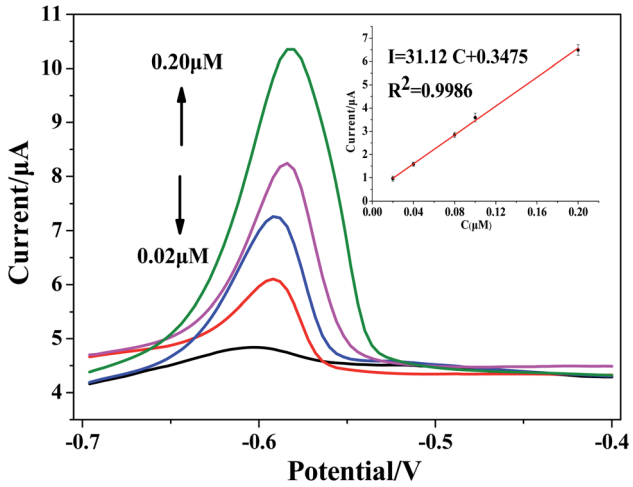

Fig. 8 SWASV response of rGO/MoS_2/CS/GCE for Pb(II) in tobacco sample, the inset was calibration curve in the range of Pb(II) concentration from 0.02 to 0.20 μM.

The stability of the sensor based on rGO/MoS_2/CS/GCE was studied through the measurements of Pb(II) (0.5 μM) for 15 days (Fig. 7 b). It illustrated that the rGO/MoS_2/CS/GCE sensor retained more than 95% of its initial signal response after 15 days, indicating that the sensor had acceptable long-term storage stability.

The electrochemical method for Pb(II) determination reported in the literature are summarized in Table S1.† Compared to these methods, our SWASV method based on rGO/MoS_2/CS/GCE had good effects in terms of detection range and LOD.

3.6 Determination of Pb(II) in tobacco leaves

In order to evaluate the practical application of rGO/MoS_2/CS/GCE, the determination for different concentrations of Pb(II) in tobacco samples (Yunnan Province, China) was conducted by standard addition method. The chemical treatment of tobacco leaves was as follows: the tobacco leaves were dried in an oven at 60 °C for 12 h and grounded into a powder. Then, 2.00 g sample was accurately put into a Teflon-lined autoclave, and 10 mL of concentrated nitric acid was added thereto for 2 hours, and placed in an oven at 120 °C for 6 hours. After cooling to room temperature, 50 mL of a solution was prepared using ultrapure water. The test solution and the acetic acid buffer solution were mixed into a 1 : 19 test solution (100 mL), and the SWASV peak current signal was determined by rGO/MoS_2/CS/GCE. Fig. 8 showed the stripping voltammetry and standard calibration plots. The linear relationship between peak current and concentration of Pb(II) was I (μA) = 31.12c (μM) + 0.3475 (R^2 = 0.9986), and the sensitivity was calculated to be 31.12 μA μM^{-1}. Based on the standard calibration equation, the amount of Pb(II) was calculated to be approximately 1.157(±0.033) μg g^{-1} in tobacco leaves. In order to verify the reliability of the experimental results, the sample was also tested by ICP-MS, and the result was 1.204 ± 0.0542 μg g^{-1}. The comparison experiment showed that the method could reliably and accurately analyze Pb(II) in actual tobacco samples.

4. Conclusions

In this work, the electrode modified by GO/MoS_2, rGO/MoS_2, rGO/MoS_2/CS nanocomposite was used to determine Pb(II) in aqueous solution, and the catalytic performance of these electrode modified materials was evaluated in details. Among them, the rGO/MoS_2/CS nanocomposites had the best electrocatalytic performance and the best sensitivity for Pb(II) detection. The sensor based on rGO/MoS_2/CS/GCE exhibited excellent performance in terms of reproducibility, stability and anti-interference ability. It has shown that LOD of the rGO/MoS_2/CS/GCE sensor was 0.0016 μM (0.33 ppb). Finally, the sensor was used to determinate Pb(II) in the actual tobacco leaves with a certain amount of ferricyanide added to reduce the influence of Cu(II), indicating that the sensor was reliable in practical applications. This work provided a new approach to the determination of Pb(II) in actual tobacco leaves samples.

Conflicts of interest

There are no conflicts to declare.

Acknowledgements

This work has been supported by the National Natural Science Foundation of China (41573103, 41340037), the Key Research and Development Program (2018GGX102004, 2018GGX104005) of Shandong Province, China.

References

1 S. Xiong, B. Yang, D. Cai, G. Qiu and Z. Wu, *Electrochim. Acta*, 2015, **185**, 52–61.
2 C. P. da Silva, T. E. de Almeida, R. Zittel, T. R. de O. Stremel, C. E. Domingues, J. Kordiak and S. X. de Campos, *Environ. Monit. Assess.*, 2018, **188**, 663.
3 T. E. Novotny, S. A. Bialous, L. Burt, C. Curtis, V. L. da Costa, S. U. Iqtidar, Y. Liu, S. Pujari and E. T. Espaignet, *Bull. W. H. O.*, 2015, **93**, 877–880.
4 S. Uhram and H. Park, *J. Ecol. Environ.*, 2017, **41**, 13.
5 Z. Mamat, H. Yimit, R. Zi A. Ji and M. Eziz, *Sci. Total Environ.*, 2014, **493**, 1098–1111.
6 L. Cai, Z. Xu, P. Bao, M. He, L. Dou, L. Chen, Y. Zhou and Y. Zhu, *J. Geochem. Explor.*, 2015, **148**, 189–195.
7 Y. Chai, J. Guo, S. Chai, J. Cai, L. Xue and Q. Zhang, *Chemosphere*, 2015, **134**, 67.
8 H. Bagheri, A. Afkhami, M. S. Tehrani and H. Khoshsafar, *Talanta*, 2012, **97**, 87–95.
9 K. Karina and R. Sitko, *Spectrochim. Acta, Part B*, 2014, **94**, 7–13.
10 M. A. Habila, *et al.*, *Clean: Soil, Air, Water*, 2016, **44**(6), 720–727.
11 T. Priya, N. Dhanalakshmi and N. Thinakaran, *Int. J. Biol. Macromol.*, 2017, **104**, 672–680.
12 S. Xiong, S. Ye, X. Hu and F. Xie, *Electrochim. Acta*, 2016, **217**, 24–33.

13 T. Yan, Z. Wang and Z. J. Pan, *Curr. Opin. Solid State Mater. Sci.*, 2018, **22**(6), 213–228.
14 H. Ge and X. Fan, *Chem. Eng. Technol.*, 2011, **34**(10), 1745–1752.
15 A. Sinha, R. Jain, H. Zhao, P. Karolia and N. Jadon, *Microchim. Acta*, 2018, **185**(2), 1–30.
16 J. Xu, Z. Cao, Y. Zhang, Z. Yuan, Z. Lou, X. Xu and X. Wang, *Chemosphere*, 2018, **195**, 351–364.
17 A. U. Rehman, M. Ikram, K. Kan, Y. Zhao, W. J. Zhang, J. Zhang and K. Shi, *Sens. Actuators, B*, 2018, **2**, 1819–1830.
18 X. Han, Z. Meng, H. Zhang and J. Zheng, *Microchim. Acta*, 2018, **185**(5), 274.
19 Z. Guo, X. K. Luo, Y. H. Li, Q. N. Zhao, M. M. Li, Y. T. Zhao, C. Ma, *et al.*, *J. Colloid Interface Sci.*, 2017, **490**, 11–22.
20 Y. Zhang, C. Zhong, Q. Zhang, B. Chen, M. He and B. Hu, *RSC Adv.*, 2015, **5**(8), 5996–6005.
21 Y. J. Choi, E. Kim, J. Han, J. H. Kim and S. Gurunathan, *Molecules*, 2016, **21**(3), 375.
22 T. B. Rouf and J. L. Kokini, *J. Mater. Sci.*, 2016, **51**(22), 9915–9945.
23 Y. Lu, X. Liang, J. Xu, Z. Zhao and G. Tian, *Sens. Actuators, B*, 2018, **273**, 1146–1155.
24 L. Fritea, M. Terti, A. Le Goff, S. Cosnier, R. Săndulescu and C. Cristea, *Procedia technology*, 2017, **27**, 106–107.
25 Z. Shariatinia and A. Bagherpour, *Powder Technol.*, 2018, **338**, 744–763.
26 H. Zhang, L. Peng, A. Chen, C. Shang, M. Lei, K. He and Q. Zeng, *Carbohydr. Polym.*, 2019, **214**, 276–285.
27 M. Zhang, F. Jia, M. Dai and S. Song, *Appl. Surf. Sci.*, 2018, **455**, 258–266.
28 H. M. Oh, H. Jeong, G. H. Han, H. Kim, J. H. Kim, S. Y. Lee and Y. H. Lee, *ACS Nano*, 2016, **10**(11), 10446–10453.
29 Y. Li, H. Wang, L. Xie, Y. Liang, G. Hong and H. Dai, *J. Am. Chem. Soc.*, 2011, **133**(19), 7296–7299.
30 K. K. H. De Silva, H. H. Huang and M. Yoshimura, *Appl. Surf. Sci.*, 2018, **447**, 338–346.
31 T. Priya, N. Dhanalakshmi, V. Karthikeyan and N. Thinakaran, *J. Electroanal. Chem.*, 2019, **833**, 543–551.
32 H. Zhang, L. Peng, A. Chen, C. Shang, M. Lei, M. He and Q. Zeng, *Carbohydr. Polym.*, 2019, **214**, 276–285.
33 X. Tan, X. Liu, W. Zeng, G. Zhao, Z. Zhang, T. Huang and L. Yang, *Anal. Chim. Acta*, 2019, **1078**, 60–69.
34 S. F. Zhou, X. J. Han, H. L. Fan, J. Huang and Y. Q. Liu, *J. Alloys Compd.*, 2018, **747**, 447–454.
35 T. Priya, N. Dhanalakshmi, V. Karthikeyan and N. Thinakaran, *J. Electroanal. Chem.*, 2019, **833**, 543–551.
36 Z. Lu, X. Lin, J. Zhang, W. Dai, B. Liu, G. Mo and J. Ye, *Electrochim. Acta*, 2019, **295**, 514–523.
37 Z. Lu, J. Zhang, W. Dai, X. Lin, J. Ye and J. Ye, *Microchim. Acta*, 2017, **184**(12), 4731–4740.